



Full length article

Manipulating the membrane penetration mechanism of helical polypeptides via aromatic modification for efficient gene delivery



Nan Zheng^{a,b,1}, Ziyuan Song^{a,1}, Jiandong Yang^{c,1}, Yang Liu^a, Fangfang Li^c, Jianjun Cheng^{a,*}, Lichen Yin^{c,*}

^a Department of Materials Science and Engineering, University of Illinois at Urbana–Champaign, 1304 W Green Street, Urbana, IL 61801, USA

^b State Key Laboratory of Fine Chemicals, Department of Polymer Science and Engineering, School of Chemical Engineering, Dalian University of Technology, Dalian 116024, PR China

^c Institute of Functional Nano & Soft Materials (FUNSOM), Jiangsu Key Laboratory for Carbon-Based Functional Materials & Devices, Collaborative Innovation Center of Suzhou Nano Science and Technology, Soochow University, Suzhou 215123, PR China

ARTICLE INFO

Article history:

Received 24 January 2017

Received in revised form 12 April 2017

Accepted 1 May 2017

Available online 3 May 2017

Keywords:

Helical polypeptide

Aromatic domain

Gene delivery

Cell penetration mechanism

Direct translocation

ABSTRACT

The delivery performance of non-viral gene vectors is greatly related to their intracellular kinetics. Cationic helical polypeptides with potent membrane penetration properties and gene transfection efficiencies have been recently developed by us. However, they suffer from severe drawbacks in terms of their membrane penetration mechanisms that mainly include endocytosis and pore formation. The endocytosis mechanism leads to endosomal entrapment of gene cargos, while the charge- and helicity-induced pore formation causes appreciable cytotoxicity at high concentrations. With the attempt to overcome such critical challenges, we incorporated aromatic motifs into the design of helical polypeptides to enhance their membrane activities and more importantly, to manipulate their membrane penetration mechanisms. The aromatically modified polypeptides exhibited higher cellular internalization level than the unmodified analogue by up to 2.5 folds. Such improvement is possibly because aromatic domains promoted the polypeptides to penetrate cell membranes via direct transduction, a non-endocytosis and non-pore formation mechanism. As such, gene cargos were more efficiently delivered into cells by bypassing endocytosis and subsequently avoiding endosomal entrapment, and the material toxicity associated with excessive pore formation was also reduced. The top-performing aromatic polypeptide containing naphthyl side chains at the incorporated content of 20 mol% revealed notably higher transfection efficiencies than commercial reagents in melanoma cells *in vitro* (by 11.7 folds) and *in vivo* (by 9.1 folds), and thus found potential utilities toward topical gene delivery for cancer therapy.

Statement of significance

Cationic helical polypeptides, as efficient gene delivery materials, suffer from severe drawbacks in terms of their membrane penetration mechanisms. The main cell penetration mechanisms involved are endocytosis and pore formation. However, the endocytosis mechanism has the limitation of endosomal entrapment of gene cargos, while the charge- and helicity-induced pore formation causes cytotoxicity at high concentrations. To address such critical issues toward the maximization of gene delivery efficiency, we incorporated aromatic domains into helical polypeptides to promote the cell membrane penetrations via direct transduction, which is a non-endocytosis and non-pore formation mechanism. The manipulation of their membrane penetration mechanisms allows gene cargos to be more efficiently delivered by bypassing endocytosis and subsequently avoiding endosomal entrapment.

© 2017 Acta Materialia Inc. Published by Elsevier Ltd. All rights reserved.

1. Introduction

Gene therapy has emerged as a promising strategy for the treatment of various genetic diseases, such as cancer, neurodegenera-

tive diseases, and immunodeficiency [1–5]. The key challenge toward successful gene therapy is the development of effective delivery systems because nucleic acids themselves cannot penetrate into cells and suffer from rapid degradation by the nucleases in the body [6–8]. While viral vectors afford high transfection efficiencies, they often suffer from serious clinical risks such as oncogenicity, immunogenicity, and insertional mutagenesis [9]. Non-viral vectors, mainly exemplified by cationic polymers

* Corresponding authors.

E-mail addresses: jianjunc@illinois.edu (J. Cheng), lcyin@suda.edu.cn (L. Yin).

¹ These authors contributed equally.

(polycations) and cationic lipids, have been considered as ideal alternatives to viral vectors because of their minimal immunogenicity, desired biocompatibility, and chemical flexibility [10–15]. However, the clinical application of non-viral vectors has been greatly hampered by their low transfection efficiencies due to the various extracellular and intracellular barriers that prevent the effective delivery of nucleic acid cargos to the target cells/organelles [16]. Among the various barriers, the biological membranes serve as a major delivery barrier against effective gene transfection. For instance, the cell membrane prevents the internalization of nucleic acids; the endosomal/lysosomal membrane prevents effective delivery into cytoplasm and thus leads to degradation of gene cargos in the lysosome; the nucleus membrane prevents DNA entry into the nuclei and thus prevents gene transcription in the nuclei [17]. As such, development of gene carriers with potent membrane activities is highly necessitated toward effective gene transfection.

Cell penetrating peptides (CPPs) are sequence-specific short oligopeptides which can mediate effective membrane penetration and translocation via either energy-dependent endocytosis or energy-independent transduction [18]. They often consist of 10–30 amino acid residues and contain a large number of positively charged amino acids such as lysine and arginine [19]. Well-known CPPs include HIV-TAT, Arg9, penetratin, and melittin. Most of the CPPs adopt inherent α -helical secondary structures, or can form trans-membrane α -helix after interacting with cell membranes, which can stabilize the membrane interactions and facilitate the cellular internalization [20,21]. Due to their excellent membrane activities, CPPs are widely utilized to facilitate the cellular delivery of a variety of exogenous materials [22]. However, when used for gene delivery, the short backbone length and insufficient cationic charge density of CPPs greatly impede their capabilities to condense and deliver genes independently [23,24]. Particularly, after complexing the gene cargos, the cationic charges and α -helical secondary structures of the short CPPs will be shielded, and thus the charge- and helix-dependent membrane activities are greatly compromised. To address such critical challenges of traditional CPPs, we recently developed cationic polypeptides with sufficiently long backbone length and stable helical structures that afford both strong membrane penetration properties and superb gene transfection efficiencies [25–28].

While the cationic helical polypeptides display excellent performance as a new category of cell penetration and gene delivery materials, they suffer from undesired drawbacks that are related to their intracellular kinetics. Particularly, the stiff helical structure allows the polypeptide to puncture pores on cell membranes, thus facilitating the direct transduction of gene cargos into cells [25–27]. However, only part of the gene cargos is internalized via such “pore formation” mechanism, while the rest of them is internalized via endocytosis, a process that leads to endosomal/lysosomal entrapment against effective gene transfection. Additionally, the charge- and helicity-induced “pore formation” mechanism will cause irreversible damage to cells when polypeptides were used at excessively high concentrations [25–27,29]. With the attempt to maximize the transfection efficiencies of helical polypeptides while minimize their toxicities, we thus seek a strategy to manipulate the membrane penetration mechanisms of helical polypeptides by promoting the non-endocytic cell uptake yet alleviating the “pore formation” mechanism.

It has been reported that hydrophobic counterions could promote the interactions of CPPs with phospholipids by coating cationic structures with lipophilic moieties as activators [30,31]. Recently, the hydrophobic domain has also been introduced into the side chains or backbones of CPPs and polymeric CPP mimics to “self-activate” their membrane penetration properties [25,32–34]. Among various hydrophobic motifs, aromatic activators have

been demonstrated to outperform aliphatic domains in enhancing membrane activities, mainly due to their flat-rigid shapes and π -electronic structures, specific interactions such as π -cation interactions, and the favorable ability to anchor proteins in the membranes [30,31]. For instance, sodium 4-(pyren-1-yl)butane-1-sulfonate exhibited better penetration enhancement than sodium dodecane-1-sulfonate [32,35]. More importantly, the direct membrane translocation of CPPs, a non-endocytic and “non-pore formation” mechanism, is closely related to the presence of aromatic domains. For instance, the incorporation of tryptophan residue into the CPP building blocks will promote their cell internalization via an energy-independent non-endocytosis pathway [36].

Based on the above understandings on the advantages of aromatic motifs, we in the current study incorporated various aromatic groups (phenyl, naphthyl, and anthryl) into the design of cationic, α -helical polypeptides, attempting to strengthen their membrane activities and potentially manipulate the membrane penetration mechanisms. To this end, random co-polypeptides bearing both charged amine groups and aromatic groups on the side chain terminals were synthesized, and we hypothesized that the aromatic domain will allow more polypeptides to penetrate cell membranes via direct transduction by bypassing the endocytic pathways. As such, they would be able to mediate effective gene delivery by minimizing the endosomal/lysosomal entrapment (Scheme 1). Additionally, due to the partial replacement of amine groups by aromatic groups, the cationic charge density of the polypeptides could be diminished, such that the excessive pore formation on cell membranes could be restricted to reduce the material toxicity. To demonstrate such hypothesis, the effect of aromatic groups on the membrane penetration potency, cell penetration mechanisms, *in vitro* and *in vivo* gene delivery efficiencies, and cytotoxicities were mechanistically explored.

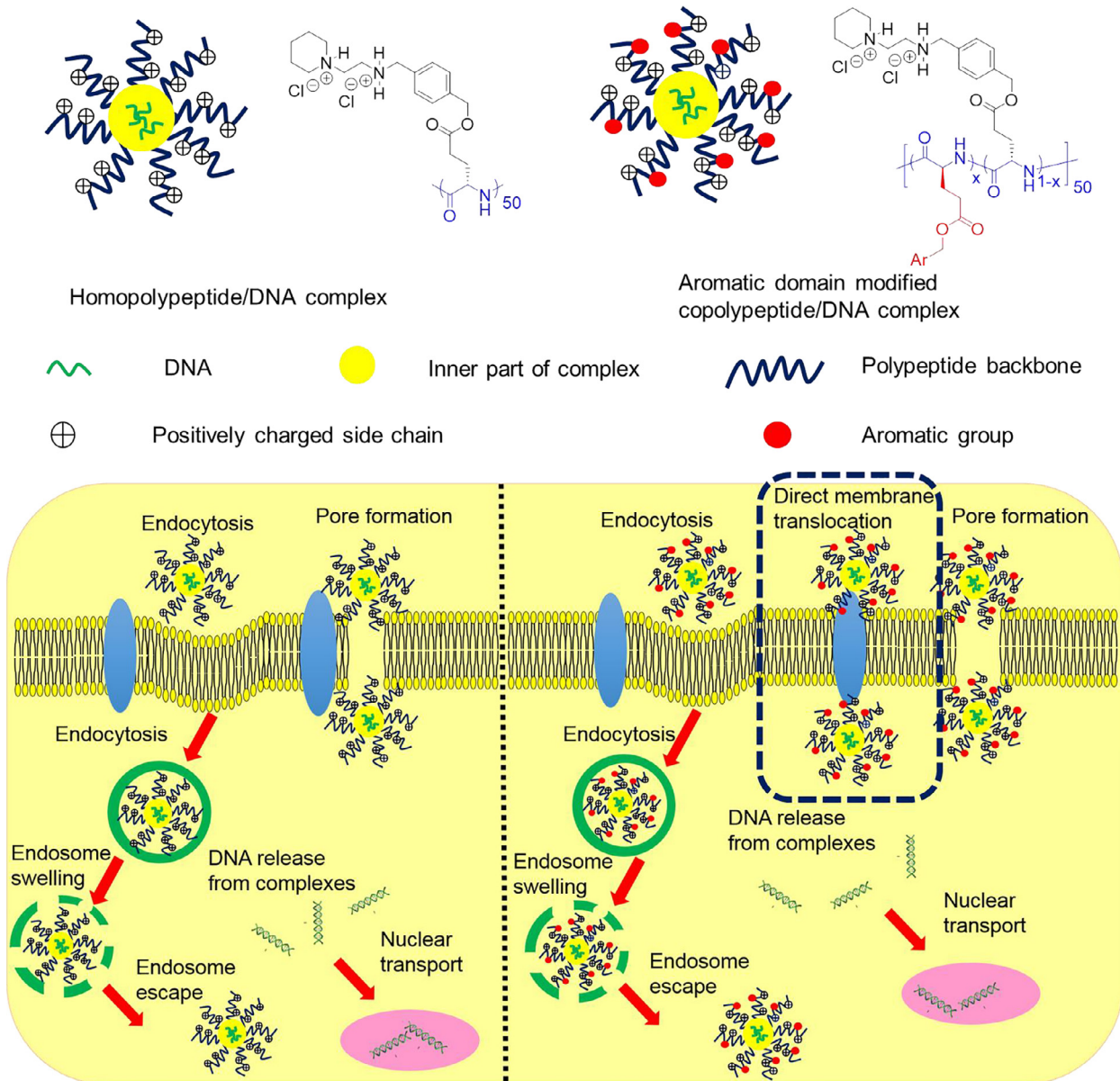
2. Materials and methods

2.1. Materials and cell lines

All chemicals were purchased from Sigma-Aldrich (St. Louis, MO, USA) and used as received unless otherwise specified. Tetrahydrofuran (THF), hexane, and dimethylformamide (DMF) were dried by a column packed with 4Å molecular sieves and stored in a glovebox. Dry nitrobenzene (NB) was prepared by treating regular NB with CaH₂ followed by distillation under reduced pressure. Hexamethyldisilazane (HMDS) and 1,5,7-triazabicyclo[4.4.0]dec-5-ene (TBD) were dissolved in anhydrous DMF in a glovebox. γ -(4-Vinylbenzyl)-L-glutamate *N*-carboxyanhydride (VB-L-Glu-NCA) was prepared as previously reported [25–27]. Pierce BCA assay kit was purchased from ThermoFisher Scientific (Rockford, IL, USA). Plasmid DNA (pDNA) encoding luciferase (pCMV-Luc) was purchased from Elim Biopharm (Hayward, CA, USA). 3-(4,5-Dimethylthiazol-2-yl)-2,5-diphenyl-2H-tetrazolium bromide (MTT) and YOYO-1 were purchased from Invitrogen (Carlsbad, CA, USA).

HeLa (human cervix adenocarcinoma cells) and B16F10 (murine melanoma cells) were purchased from the American Type Culture Collection (Rockville, MD, USA) and were cultured in Dulbecco's Modified Eagle Medium (DMEM) (Gibco, Grand Island, NY, USA) containing 10% fetal bovine serum (FBS) and 1% penicillin-streptomycin.

Female C57BL/6 mice (8–10 week old) were obtained from Charles River Laboratory (Wilmington, MA, USA) and were housed in a germ-free environment with four mice per cage. Mice were given access to food and water and exposed to a 12:12 h light–dark cycle (7:00 am–7:00 pm) at 25 ± 1 °C. The animal experimental protocol was approved by the Institutional Animal Care and Use



Scheme 1. Schematic illustration of cell penetration and intracellular DNA delivery mediated by helical polypeptide nanoparticles.

Committees (IACUC) of University of Illinois at Urbana-Champaign.

2.2. Instrumentation

^1H NMR spectra were recorded on a Varian UI500NB MHz spectrometer. Chemical shifts were reported in ppm and referenced to the solvent proton impurities. Gel permeation chromatography (GPC) experiments were performed on a system equipped with an isocratic pump (Model 1100, Agilent Technology, Santa Clara, CA, USA), a DAWN HELEOS multi-angle laser light scattering (MALLS) detector (Wyatt Technology, Santa Barbara, CA, USA), and an Optilab rEX refractive index detector (Wyatt Technology, Santa Barbara, CA, USA). Separations were performed using serially connected size exclusion columns (10^2 Å, 10^3 Å, 10^4 Å, 10^5 Å, and 10^6 Å Phenogel columns, 5 mm, 300×7.8 mm, Phenomenex, Torrance, CA, USA) at 60°C with DMF containing 0.1 M LiBr as the mobile phase. The detection wavelength was set at 658 nm, and the MALLS detector was calibrated using pure toluene, which

allowed determination of the absolute molecular weights (MWs) instead of calibration using polymer standards. The MWs of polypeptides were calculated according to the dn/dc value of each polymer sample calculated offline by using the internal calibration system processed by the ASTRA V software (version 6.1.1.17, Wyatt Technology, Santa Barbara, CA, USA). Circular dichroism (CD) measurements were carried out on a JASCO J-815 CD spectrometer (JASCO, Easton, MD, USA). Polypeptide was dissolved in DI water at a concentration of 0.2 mg/mL at pH = 7, and was placed in a quartz cell with a pathlength of 0.1 cm. The mean residue molar ellipticity and helicity of each polymer were calculated based on the measured apparent ellipticity following the reported formula [27]:

$$\text{Ellipticity } ([\theta], \text{deg cm}^2 \text{ dmol}^{-1}) = \frac{\text{millidegree} \times \text{mean residue weight}}{\text{pathlength (mm)} \times \text{concentration (mg mL}^{-1})}$$

$$\text{Helicity } (\%) = \frac{-[\theta_{222}] + 3000}{39000} \times 100$$

2.3. Synthesis of γ -benzyl-L-glutamate based *N*-carboxyanhydride (B-L-Glu-NCA), γ -naphthyl-L-glutamate based *N*-carboxyanhydride (Naph-L-Glu-NCA), γ -anthryl-L-glutamate based *N*-carboxyanhydride (Anth-L-Glu-NCA), and L-leucine based *N*-carboxyanhydride (L-Leu-NCA)

Aromatic domain modified glutamate was synthesized according to the literature procedure [37] (Scheme S1). *N,N,N',N'*-Tetramethylguanidine (8.5 mL, 67.8 mmol) was added slowly to a mixture of L-glutamic acid (5.00 g, 34.0 mmol), L-glutamic acid copper (II) complex copper (II) salt (8.63 g, 16.8 mmol), DMF (32.0 mL), and water (4.75 mL). After all solid was dissolved, 1-(chloromethyl)naphthalene (10.0 mL, 71.0 mmol) was added in one portion and the resulting mixture was heated at 40 °C for 24 h. Acetone (300 mL) was then added and the reaction mixture was further stirred for another 20 h to get a fine precipitate. The precipitate was filtered, washed twice with acetone, and then added into a fresh EDTA disodium salt aqueous solution. After stirring at RT for 20 h, the crude product was collected by filtration and washed three times with water. The product γ -naphthyl-L-glutamate (Naph-L-Glu) was obtained as white powder after recrystallization from isopropanol-water (50 mL, 1:1, v/v) (68% yield). ¹H NMR (500 MHz, DMSO-*d*₆:DCI-D₂O (9:1, v/v), δ): 7.93 (m, 3H, ArH), 7.52 (m, 4H, ArH), 5.57 (m, 2H, ArCH₂O-), 3.89 (t, 1H, α -H), 2.63–2.43 (m, 2H, -COCH₂CH₂-), 2.05 (m, 2H, -COCH₂-CH₂-).

γ -Anthryl-L-glutamate (Anth-L-Glu) was synthesized with the same method using 9-(chloromethyl)anthracene as the electrophile (63% yield). ¹H NMR (500 MHz, DMSO-*d*₆:DCI-D₂O (9:1, v/v), δ): 8.64 (d, 1H, ArH), 8.26 (d, 2H, ArH), 8.06 (d, 2H, ArH), 7.55 (t, 2H, ArH), 7.48 (t, 2H, ArH), 6.04 (s, 2H, ArCH₂O-), 3.84 (t, 1H, α -H), 2.54–2.34 (m, 2H, -COCH₂CH₂-), 2.00 (m, 2H, -COCH₂-CH₂-).

NCA monomer was synthesized through ring-closing reaction of amino acid with phosgene (Scheme S1). In a dried 250 mL two-neck round bottom flask, Naph-L-Glu (0.86 g, 3.00 mmol) was added and dried under vacuum for 2 h. Anhydrous THF (30.0 mL) was then added to the flask along with phosgene solution (10% in toluene, 3.9 mL, 3.6 mmol). The mixture was kept stirring at 50 °C for 2 h under the protection of drying tube. The solvent and excessive phosgene was then removed under vacuum to obtain a yellow solid. The product γ -naphthyl-L-glutamate based *N*-carboxyanhydride (Naph-L-Glu-NCA) was obtained as light yellow crystal after recrystallization from THF-hexane (1:5, v/v) three times in a glovebox (86% yield). ¹H NMR (500 MHz, CDCl₃, δ): 7.89 (m, 3H, ArH), 7.53 (m, 4H, ArH), 7.45 (t, 1H, ArH), 6.53 (s, 1H, ring N-H), 5.61 (m, 2H, ArCH₂O-), 4.34 (t, 1H, α -H), 2.60 (m, 2H, -COCH₂CH₂-), 2.38–2.04 (m, 2H, -COCH₂CH₂-).

γ -Benzyl-L-glutamate-based *N*-carboxyanhydride (B-L-Glu-NCA) was synthesized with the same method using commercially available γ -benzyl-L-glutamate (79% yield). ¹H NMR (500 MHz, CDCl₃, δ): 7.36 (m, 5H, ArH), 6.76 (s, 1H, ring N-H), 5.13 (m, 2H, ArCH₂O-), 4.38 (t, 1H, α -H), 2.59 (m, 2H, -COCH₂CH₂-), 2.35–2.07 (m, 2H, -COCH₂CH₂-).

γ -Anthryl-L-glutamate-based *N*-carboxyanhydride (Anth-L-Glu-NCA) was synthesized with the same method using Anth-L-Glu (89% yield). ¹H NMR (500 MHz, CDCl₃, δ): 8.53 (d, 1H, ArH), 8.31 (d, 2H, ArH), 8.04 (d, 2H, ArH), 7.60 (t, 2H, ArH), 7.51 (t, 2H, ArH), 6.21 (m, 3H, ring N-H and ArCH₂O-), 4.32 (t, 1H, α -H), 2.56 (m, 2H, -COCH₂CH₂-), 2.31–2.04 (m, 2H, -COCH₂CH₂-).

L-Leucine-based *N*-carboxyanhydride (L-Leu-NCA) was synthesized with the same method using commercially available L-leucine (79% yield). ¹H NMR (500 MHz, CDCl₃, δ): 7.25 (s, 1H, ring N-H), 4.35 (m, 1H, α -H), 1.80 (m, 2H, -CH₂CH(CH₃)₂), 1.68 (m, 1H, -CH(CH₃)₂), 0.97 (dd, 6H, -CH(CH₃)₂).

2.4. Synthesis of poly(γ -4-((2-(piperidin-1-yl)ethyl)amino)methyl)benzyl-L-glutamate) (PPABLG, **P0**), PPABLG random copolymers with hydrophobic aromatic residues (**P1** to **P6**), and PPABLG random copolymers with hydrophobic aliphatic residues (**P7** and **P8**)

PPABLG (**P0**) was synthesized according to the reported procedure [26]. ¹H NMR (500 MHz, TFA-*d*, δ): 7.98–7.33 (m, 4H, ArH), 5.46 (br s, 2H, ArCH₂O-), 5.06 (br s, 2H, ArCH₂NH-), 4.67 (s, 1H, α -H), 4.40–3.79 (m, 6H, -NH⁺CH₂CH₂NH₂⁺- and -NH⁺CH₂CH₂CH₂CH₂-CH₂-), 3.26 (s, 2H, -NH⁺CH₂CH₂NH₂⁺-), 2.92 (s, 2H, -COCH₂CH₂-), 2.73–1.60 (m, 8H, -COCH₂CH₂- and -NH⁺CH₂CH₂CH₂CH₂CH₂-).

A representative synthetic procedure of hydrophobic groups modified PPABLG random copolymers was shown as follows (take PBLG_{10-r}-PPABLG₄₀ as an example). In a glovebox, VB-L-Glu-NCA (58 mg, 0.20 mmol) and B-L-Glu-NCA (13 mg, 0.05 mmol) were dissolved in DMF (1.50 mL), followed by the addition of nitrobenzene (60 μ L), HMDS (0.1 M in DMF, 50 μ L, M/I = 50) and TBD (0.01 M in DMF, 50 μ L). The polymerization solution was stirred at RT until the conversion was above 99% monitored by FTIR. Methanol (100 μ L), benzyl chloroformate (50 μ L), and *N,N*-diisopropylethylamine (50 μ L) were added to the solution and the resulting mixture was stirred for 3 h to protect the terminal amino groups. The obtained copolymer poly(γ -benzyl-L-glutamate)-*random*-poly(γ -4-vinylbenzyl)-L-glutamate) (PBLG-*r-r*-PVBLG) was precipitated using hexane/ether (1:1, v/v) and collected by centrifuge (85%–90% yield).

PBLG-*r-r*-PVBLG copolymer (54 mg) was then dissolved in chloroform (30 mL) and oxidized by O₃ at -78 °C. Dimethyl sulfide (1.0 mL) was added and the solution was stirred at RT overnight before the solvent was removed under vacuum. The product poly(γ -benzyl-L-glutamate)-*random*-poly(γ -4-aldehydobenzyl)-L-glutamate) (PBLG-*r-r*-PABLG) was precipitated using methanol and collected by centrifugation (81% yield). The actual random copolymer composition was quantified using the integration ratio of the α -protons in PBLG residues to the α -protons in PABLG residues from ¹H NMR.

The resulting PBLG-*r-r*-PABLG copolymer (43 mg, 0.13 mmol aldehyde groups) was then dissolved in DMF (2 mL), where 1-(2-aminoethyl)piperidine (184 μ L, 1.30 mmol) was added and the solution was stirred at 50 °C for 24 h. Borane (8 M in the form as pyridine complex, 163 μ L, 1.30 mmol) was then added, and the resulting solution was further stirred at 50 °C for another 24 h. HCl (5 M, 1.0 mL) was added to the solution to quench the excessive borane, and the polymer was then purified by dialysis against DI water for 3 days (molecular weight cut-off = 1 kDa). The final polymer PBLG-*r-r*-PPABLG (**P1**) was obtained as white powder after lyophilization (60% yield for ozonolysis and reductive amination). ¹H NMR (500 MHz, TFA-*d*, δ): 7.99–7.44 (m, 21H, ArH), 5.44 (br s, 10H, ArCH₂O-), 5.03 (s, 8H, ArCH₂NH-), 4.68 (s, 5H, α -H), 4.38–3.84 (m, 24H, -NH⁺CH₂CH₂NH₂⁺- and -NH⁺CH₂CH₂CH₂CH₂CH₂-), 3.27 (s, 8H, -NH⁺CH₂CH₂NH₂⁺-), 2.92 (s, 10H, -COCH₂CH₂-), 2.71–1.62 (m, 34H, -COCH₂CH₂- and -NH⁺CH₂CH₂CH₂CH₂CH₂-).

P2 to **P8** were synthesized by the similar method starting from different NCA monomers and different M/I feeding ratios (60–70% yield for ozonolysis and reductive amination), and their compositions were shown in Table 1.

2.5. Cell penetration efficiency of polypeptides

HeLa cells were seeded on 96-well plates at 1 \times 10⁴ cells/well and cultured for 24 h. The medium was refreshed with opti-MEM into which RhB-labeled polypeptides were added at 2 μ g/well. After incubation at 37 °C for 4 h, the cells were washed with cold PBS containing 20 U/mL heparin for three times, which could remove surface-bound cationic materials from cells [38]. Cells

Table 1
Structures and characterizations of random co-polypeptides.^a

Name	Hydrophobic domain	M/I ^b	M _n (M _n [*]) (kDa) ^{c,d}	PDI ^d	Composition ^e
P0	–	(50 + 0)/1	25.0 (23.9)	1.13	PPABLG ₅₂
P1	Phenyl	(10 + 40)/1	22.6 (21.4)	1.08	PBLG _{9-r} -PPABLG ₄₃
P2	Phenyl	(25 + 25)/1	17.3 (17.8)	1.10	PBLG _{27-r} -PPABLG ₂₄
P3	Naphthyl	(10 + 40)/1	25.4 (21.9)	1.06	PNLG _{12-r} -PPABLG ₄₆
P4	Naphthyl	(25 + 25)/1	19.0 (19.0)	1.17	PNLG _{25-r} -PPABLG ₂₅
P5	Anthryl	(10 + 40)/1	21.2 (22.4)	1.20	PALG _{9-r} -PPABLG ₃₈
P6	Anthryl	(25 + 25)/1	20.9 (20.3)	1.09	PALG _{24-r} -PPABLG ₂₇
P7	Isopropyl	(10 + 40)/1	23.5 (20.7)	1.12	PLLeu _{13-r} -PPABLG ₄₅
P8	Isopropyl	(25 + 25)/1	14.1 (15.8)	1.07	PLLeu _{26-r} -PPABLG ₂₁

^a All polymerizations are carried out at RT in a glovebox for 24 h.

^b Feed ratio of (NCA containing hydrophobic domains + VB-I-Glu-NCA)/HMDS.

^c Obtained molecular weight (expected molecular weight).

^d Determined by GPC.

^e Determined by ¹H NMR. The abbreviations of polymers were shown in Scheme 2.

were then lysed with RIPA lysis buffer (100 μL/well) at RT for 20 min before assessment of fluorescent content by spectrofluorimetry ($\lambda_{\text{ex}} = 540$ nm, $\lambda_{\text{em}} = 625$ nm) and protein level using the BCA kit. The cell penetration level was expressed as μg RhB-labeled polypeptide associated with 1 mg of cellular protein.

2.6. Characterization of polypeptide/DNA complexes

Gel retardation assay was used to evaluate the DNA condensation. Polypeptide/DNA complexes at various weight ratios were loaded on a 1% agarose gel at 100 ng DNA/well followed by electrophoresis at 100 V for 45 min. Naked DNA was used as a control, and DNA migration in the agarose gel was visualized by a Gel Doc imaging system (Biorad, Hercules, CA, USA). EB exclusion assay was performed to quantify the DNA condensation as follows. DNA was stained with EB at the DNA/EB weight ratio of 10 at RT for 1 h. Then the polypeptides were added into the DNA/EB solutions at determined weight ratios followed by further incubation at RT for 30 min before evaluation by fluorescence intensity ($\lambda_{\text{ex}} = 510$ nm, $\lambda_{\text{em}} = 590$ nm). The DNA condensation efficiency (%) was calculated according to the following equation:

$$\text{DNA condensation efficiency (\%)} = \left(1 - \frac{F - F_{\text{EB}}}{F_0 - F_{\text{EB}}}\right) \times 100$$

where F_{EB} , F , and F_0 denote the fluorescence intensity of pure EB solution, DNA/EB solution with polypeptide, and DNA/EB solution without any polypeptide, respectively.

Particle size and zeta potential of polypeptide/DNA complexes at various weight ratios were evaluated by dynamic laser scattering (DLS) on a Malvern Zetasizer (Herrenberg, Germany).

2.7. Cell uptake of polypeptide/DNA complexes

DNA was labeled with YOYO-1 at one dye molecule per 50 bp DNA. The obtained YOYO-1-DNA was allowed to form complexes with polypeptides as described above. HeLa cells were seeded on 96-well plates at 1×10^4 cells/well and cultured for 24 h. The cell culture medium was refreshed with opti-MEM (100 μL/well) into which the complexes were added at 0.1 μg DNA/well. After incubation at 37 °C for 4 h, cells were washed with PBS containing heparin (20 U/mL) for three times and subsequently lysed with the RIPA lysis buffer (100 μL/well) at RT for 20 min before assessment of the YOYO-1-DNA content by spectrofluorimetry ($\lambda_{\text{ex}} = 485$ nm, $\lambda_{\text{em}} = 530$ nm) and the protein level using the BCA kit. The cell uptake level was expressed as ng YOYO-1-DNA associated with 1 mg of cellular protein.

2.8. Cell penetration and DNA internalization mechanisms

To explore the involvement of the energy-dependent endocytosis pathway, HeLa cells were cultured on 96-well plates and incubated with RhB-labeled polypeptides or polypeptide/YOYO-1-DNA complexes for 4 h at 37 °C or 4 °C as described above. Results were expressed as the percentage level at 4 °C normalized by that at 37 °C. In a further study, the cellular internalization level in the presence of various endocytic inhibitors was evaluated. Particularly, HeLa cells cultured on 96-well plates were pre-incubated with endocytic inhibitors including methyl-β-cyclodextrin (mβCD, 5 mM), wortmannin (10 μg/mL), and chlorpromazine (10 μg/mL) for 30 min prior to the addition of RhB-labeled polypeptides as described above. After incubation at 37 °C for 2 h, the cellular uptake level of RhB-labeled polypeptides was quantified, and results were expressed as percentage uptake level of control cells that were treated with RhB-labeled polypeptides in the absence of endocytic inhibitors for 2 h.

2.9. Polypeptide-mediated pore formation activity

The capability of polypeptides to induce pore formation on cell membranes was evaluated in terms of the cell uptake level of a hydrophilic, membrane-impermeable dye, fluorescein isothiocyanate (FITC) in its non-reactive form (fluorescein-tris(hydroxy methyl)methanethiourea, FITC-Tris) [22]. Briefly, cells were seeded on 96-well plates at 1×10^4 cells/well and cultured for 24 h. The medium was replaced with Opti-MEM (100 μL/well) into which polypeptides and FITC-Tris were added at 2 μg/well and 0.2 μg/well, respectively. Free FITC-Tris without polypeptides was added as a control. After incubation at 37 °C for 2 h, cells were washed with PBS containing heparin (20 U/mL) for three times and then lysed with the RIPA lysis buffer (100 μL/well). The FITC-Tris content in the lysate was quantified using spectrofluorimetry ($\lambda_{\text{ex}} = 485$ nm, $\lambda_{\text{em}} = 530$ nm), and the protein level was determined using the BCA kit. Uptake level was expressed as ng FITC-Tris associated with 1 mg of cellular protein.

2.10. Confocal laser scanning microscopy (CLSM) observation

HeLa cells incubated in serum-free DMEM in a 6-well plate were treated with RhB-P0 and RhB-P3 at 10 μg/well. Following incubation at 37 °C or 4 °C for 2 h, cells were washed with PBS containing heparin (20 U/mL) for 3 times, fixed with paraformaldehyde (4%), stained with DAPI (2 μg/mL), and subjected to observation using CLSM (LSM700, Zeiss, Germany). To evaluate the endosomal entrapment and escape of DNA cargos, HeLa cells were incubated with P3/YOYO-1-DNA and P0/YOYO-1-DNA com-

plexes (1 μg of YOYO-1-DNA/well) at 37 °C for 4 h. Cells were then washed with PBS containing heparin (20 U/mL) three times, fixed with paraformaldehyde (4%), stained with Hoechst33258 (2 $\mu\text{g}/\text{mL}$) and LysoTracker Red[®] (200 nM) according to the manufacturer's protocol, and visualized by CLSM (LSM700, Zeiss, Germany). To quantify the endosomal escape ratio of YOYO-1-DNA, the colocalization ratio between YOYO-1-DNA and LysoTracker Red was quantified as follows using the ImageJ software:

$$\text{Colocalization ratio (\%)} = \frac{\text{DNA pixels}_{\text{colocalization}}}{\text{DNA pixels}_{\text{total}}} \times 100$$

where DNA pixels_{colocalization} represents the number of YOYO-1-DNA pixels colocalizing with LysoTracker Red, and DNA pixels_{total} represents the number of all YOYO-1-DNA pixels in the CLSM images. Results were presented as the mean of twenty individual cells.

2.11. Cytotoxicity measurement

HeLa or B16F10 cells were seeded on 96-well plates at 1×10^4 cells/well and cultured for 24 h or 48 h until they reached confluence. The medium was replaced by Opti-MEM (100 $\mu\text{L}/\text{well}$) into which the polypeptide or polypeptide/DNA complexes were added at various polypeptide final concentrations (100, 50, 20, 10 $\mu\text{g}/\text{mL}$). After incubation at 37 °C for 4 h, the medium was refreshed with serum-containing media and further incubated for 20 h before the assessment of cell viability using the MTT assay. The results were expressed as percentage viability of control cells.

2.12. In vitro transfection

HeLa or B16F10 cells were seeded on 96-well plates at 1×10^4 cells/well and incubated until cells reached 70% confluence. The medium was replaced by Opti-MEM or fresh DMEM containing 10% serum, into which polypeptide/DNA complexes at various weight ratios were added at 0.2 μg DNA/well. After incubation for 4 h, the complexes were removed and fresh media were added. Cells were further cultured for 20 h before quantification of luciferase expression level using a Bright-Glo Luciferase assay kit (Promega, Madison, USA) and cellular protein level using a BCA kit. Results were expressed as relative luminescence unit (RLU) associated with 1 mg of cellular protein.

2.13. In vivo transfection

Female C57/BL6 mice (18–20 g) were unshaved, anesthetized by isoflurane, and subcutaneously injected with 1×10^7 B16F10 cells in the right flank. When the tumor sizes reached 100 mm^3 (measured by a vernier caliper), mice were randomly divided into six groups (four mice per group), anesthetized, and intratumorally injected with **P3**/DNA complexes (w/w = 10), **P0**/DNA complexes (w/w = 10), polyethylenimine (PEI, 25 kDa)/DNA complexes (w/w = 1), PLL/DNA complexes (w/w = 3), naked DNA, and HEPES buffer containing glucose (HBG, 20 mM HEPES, pH = 7.2, 5% glucose) at 10 μg pCMV-Luc DNA/injection/mouse (injection volume 50 μL) for three times with 4 h spaced between each injection (total dose of 30 μg DNA/mouse). Polymer/DNA complexes were freshly prepared in HBG before injection. Forty-eight hours post injection, mice were sacrificed. Tumor tissues were harvested and homogenized with the passive cell lysis buffer (Promega, Madison, USA) containing protease inhibitor cocktail. The mixture was frozen in liquid nitrogen and thawed in water bath (37 °C) for three cycles. After centrifugation at 4 °C and 12,000 rpm for 10 min, the supernatant was collected and quantified in terms of luciferase activity and protein content as described above. The transfection efficiency was expressed as RLU/mg protein.

To evaluate the intracellular distribution of polyplexes containing Cy5-labeled DNA after intratumoral injection, mice bearing B16F10 xenograft tumors were anesthetized and intratumorally injected with **P3**/Cy5-DNA complexes (w/w = 10), naked DNA, and HBG at 10 μg Cy5-DNA/mouse (injection volume 50 μL). Four hours post injection, tumors were harvested, embedded in the OTC compound, and 10- μm thick tissues slices were obtained on a cryostat. After staining with DAPI (2 $\mu\text{g}/\text{mL}$), the tissue slices were visualized by CLSM (LSM700, Zeiss, Germany).

2.14. Statistical analysis

Statistical analysis was performed using Student's *t*-test and differences were judged to be significant at **p* < 0.05 and very significant at ***p* < 0.01.

3. Results and discussion

3.1. Synthesis and characterization of aromatically modified helical polypeptides

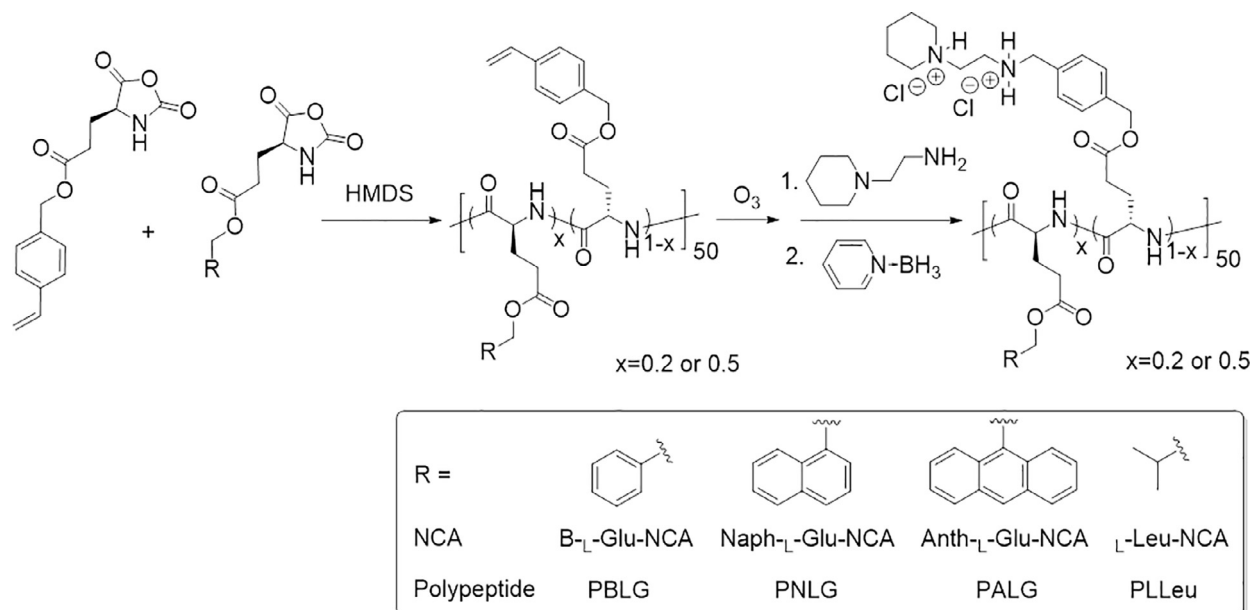
To enable the preparation of aromatically modified polypeptides, *N*-carboxyanhydrides (NCAs) with aromatic domains (phenyl, naphthyl, and anthryl) were first synthesized and characterized (Supplementary Scheme S1). The aromatic NCAs were then allowed to copolymerize with VB-L-Glu-NCA through HMDS-initiated controlled ring-opening polymerization (ROP) followed by side-chain ozonolysis and reductive amination [26], ultimately obtaining the cationic, helical random co-polypeptides containing both aromatic groups and amine groups on side-chain terminals (Scheme 2). As a control, leucine was also incorporated as a hydrophobic yet aliphatic residue in the final cationic, helical random co-polypeptides (Scheme 2).

By incorporating various hydrophobic groups including benzyl, naphthyl, anthryl, and isopropyl (non-aromatic) groups into the homo-polypeptide PPABLG (**P0**) at the content of 20 mol% and 50 mol%, we developed a small library of co-polypeptides with various charge densities and hydrophobic domains, named as **P1** to **P8** (Table 1). All random copolymers have well-defined structures, as evidenced by the controlled MWs, low PDI (<1.2), and predictable composition tuned by the monomer feeding ratios (Table 1).

The secondary structures of the polypeptides were then evaluated by CD. All of the random co-polypeptides adopted typical α -helical structures with 60–85% helicity as demonstrated by the characteristic ellipticity minima at 208 and 222 nm (Fig. 1A; Supplementary Table S1). It thus substantiated that the introduction of aromatic/aliphatic domains to the side chain terminals of polypeptides did not compromise their helical structures. In our previous studies, we have demonstrated that the cationic helical polypeptide (**P0**) could maintain stable helical structure upon treatment with trypsin, which indicated desired stability of the polypeptide against proteolytic degradation [39]. Such stability could be explained by the composition of the NCA-polymerized polypeptide that does not contain natural amino acids, and thus does not provide an effective cutting site for naturally occurring proteases [40]. Additionally, the helical polypeptides possess long hydrophobic side chains, which leads to the embedment of polypeptide backbone within the center and thus enzymes with large molecular sizes cannot easily access the backbone to achieve effective cutting.

3.2. Cell penetration properties and mechanisms

To evaluate their cell penetration properties, polypeptides were covalently labeled with Rhodamine B (RhB) and were incubated



Scheme 2. Synthetic routes of cationic, α -helical random co-polypeptides modified with hydrophobic domains (**P1–P8**).

with HeLa cells at 37 °C for 4 h before quantification of the internalization level by spectrofluorimetry. As shown in Fig. 1C, all the aromatically modified polypeptides (**P1–P6**) showed notably

higher cellular internalization levels than their unmodified analogue (**P0**) by up to 2.5 folds, which indicated that the incorporation of aromatic residues greatly enhanced their membrane

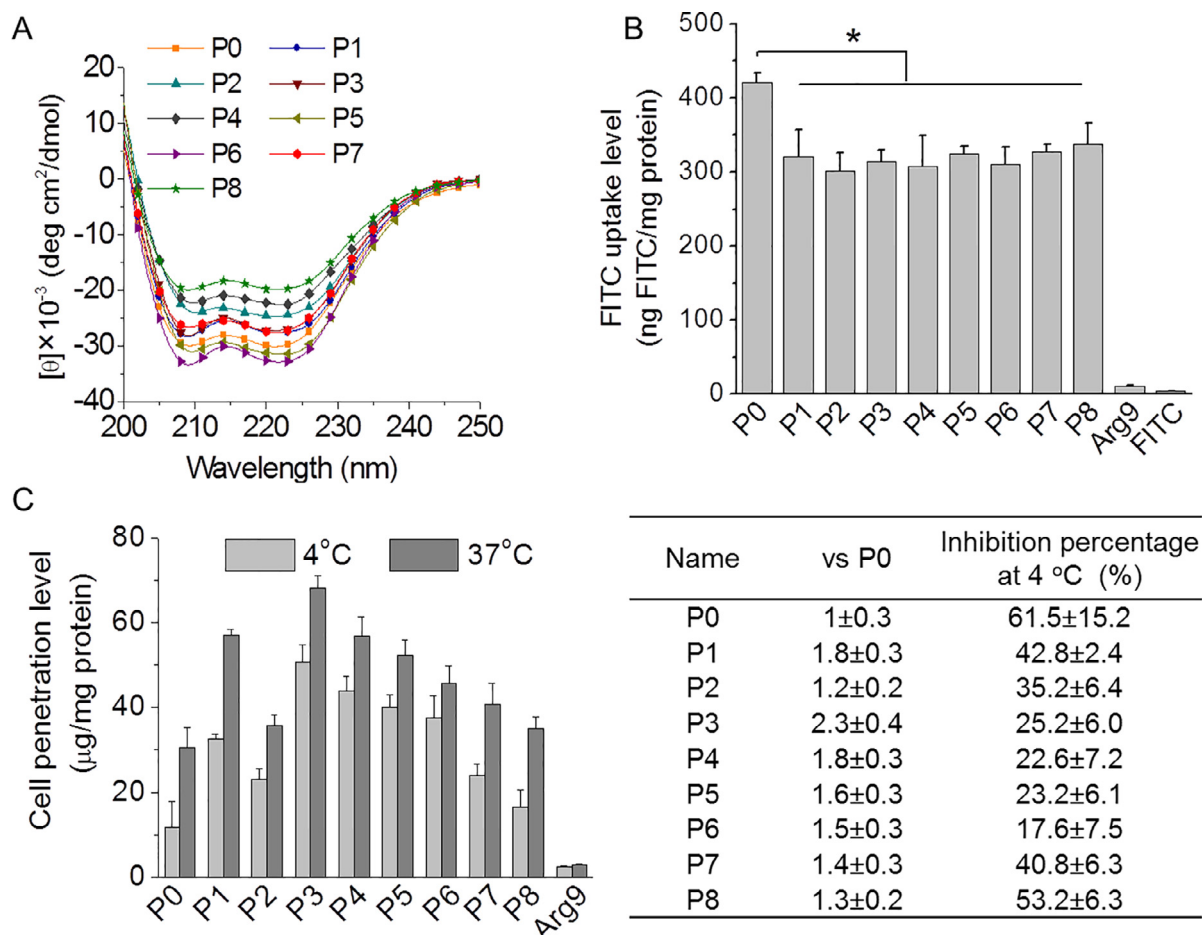


Fig. 1. (A) CD spectra of **P0** to **P8** in DI water at pH 7.0 (0.1 mg/mL). (B) FITC-Tris uptake level in HeLa cells following co-incubation with polypeptides for 2 h at 37 °C (n = 3). (C) Cell penetration levels of RhB-labeled polypeptides in HeLa cells (left), the fold of increment over **P0** in terms of the penetration level, and inhibition percentage at 4 °C (right) (n = 3).

penetration capabilities. When compared to their analogues bearing the isopropyl (hydrophobic and aliphatic) side groups (**P7** and **P8**), aromatic polypeptides also showed significantly higher membrane activities, which suggested that apart from hydrophobicity, the introduced aromaticity greatly contributed to the membrane activities, mainly because the aromatic residues have more favorable free energies of internalization into the cell bilayer membrane. An increase in the aromatic content from 20 mol% to 50 mol% led to a significant decrease in the penetration level, which could be attributed to the excessive loss of positive charges on polypeptides that hampered the electrostatic interactions between positively charged polypeptides and negatively charged phospholipid bilayers in cell membranes. Among all the co-polypeptides, **P3** with 20 mol% of naphthyl side terminal groups exhibited the highest penetration levels in HeLa cells, which was 25 fold higher than Arg9, a widely recognized CPP.

To further evaluate the involvement of endocytosis during polypeptide-assisted membrane penetration, we further evaluated the cellular uptake level of RhB-labeled polypeptides in HeLa cells following incubation at 4 °C for 4 h, when the energy-dependent endocytosis pathway is completely blocked. As shown in Fig. 1C, the uptake level of un-modified **P0** was remarkably inhibited by 61% at 4 °C compared to that at 37 °C, suggesting that it penetrated into cells mainly through endocytosis. In huge difference to **P0**, the uptake level of aromatically modified polypeptides (**P1–P6**) was inhibited by only 18 ~ 43%, indicating that aromatic side groups allowed more polypeptides to penetrate cell membranes via non-endocytic pathways. CLSM observation also revealed extensive intracellular fluorescence of RhB-**P3** following incubation at 4 °C in comparison to the remarkable reduction in the intracellular fluorescence of RhB-**P0** at 4 °C (Supplementary Fig. S1). Endosomal entrapment following the endocytosis mechanism represents one of the most critical barriers against effective intracellular delivery, because the cargo molecules will not have the chance to reach the targeted sub-cellular compartment to exert biological/pharmacological functions unless they afford an effective strategy to escape from endosomes/lysosomes [30,31]. In this regard, the aromatic polypeptides featuring non-endocytic cell penetration capabilities would find promising potentials for effective intracellular delivery of cargo molecules. **P7** and **P8** that bear the hydrophobic yet non-aromatic isopropyl groups showed relatively higher inhibition rates at 4 °C in terms of the cell penetration levels, which again highlighted the importance of aromaticity in mediating non-endocytic membrane penetration. This result was also proved by the cell penetration level in the presence of various endocytosis inhibitors (Supplementary Fig. S2).

Because helical polypeptides have been previously demonstrated to mediate non-endocytic membrane penetration via the “pore formation” mechanism [25–27], we thus further explored the effect of aromatic modification on the pore formation capabilities of helical polypeptides by evaluating the cellular uptake level of a membrane-impermeable dye, FITC in its non-reactive form, FITC-Tris [22]. Free FITC-Tris cannot be taken up by HeLa cells while the pre-treatment of helical polypeptides led to a significant increase of FITC-Tris uptake level (Fig. 1B), indicating that the helical polypeptides were able to puncture pores on the cell membranes to allow direct diffusion of FITC-Tris into the cells. All the aromatically modified polypeptides revealed significantly lower FITC-Tris uptake level than their un-modified analogue **P0**, which could be ascribed to the partial replacement of amine groups by aromatic domains that diminished the cationic charge densities on polypeptide structures to weaken the pore formation potency. In combination with the remarkably improved membrane penetration properties yet reduced pore formation potency of aromatic polypeptides, it was suggested that aromatic domains may promote the polypeptides to direct translocate across cell membranes, an efficient, non-endocytosis pathway other than the “pore formation” mechanism that numerous CPPs utilize to enter cells. In support of such hypothesis, random coiled analogues of **P0** and **P3** were synthesized via polymerization of the racemic DL-NCA (termed as **P0(DL)** and **P3(DL)**, respectively), and their cellular uptake levels as well as pore formation capabilities were further assessed. Because of their random-coiled conformation (Fig. 2A), the helicity-associated pore formation property was deprived (Fig. 2C). **P0(DL)** showed minimal uptake level at both 37 °C and 4 °C, indicating its impotency to penetrate membranes via direct translocation. Comparatively, **P3(DL)** showed notably higher uptake level than **P0(DL)** at 37 °C and 4 °C, and its uptake level was inhibited by only 25% at 4 °C compared to that at 37 °C (Fig. 2B), which again demonstrated that the aromatic side terminal groups greatly contributed to the membrane penetration capabilities of polypeptides via the direct translocation mechanism rather than the pore formation mechanism.

3.3. Aromatic polypeptide-mediated gene delivery in vitro

The capabilities of aromatic helical polypeptides to mediate gene delivery were evaluated with plasmid DNA (pDNA) encoding luciferase (pCMV-Luc) as the reporter gene. Because of their polycationic nature, all the polypeptides were able to condense the anionic pDNA at the polypeptide/DNA weight ratios higher than 8 (Supplementary Figs. S3 and S4) as evidenced by the gel retardation assay and EB exclusion assay. Upon complete condensation of

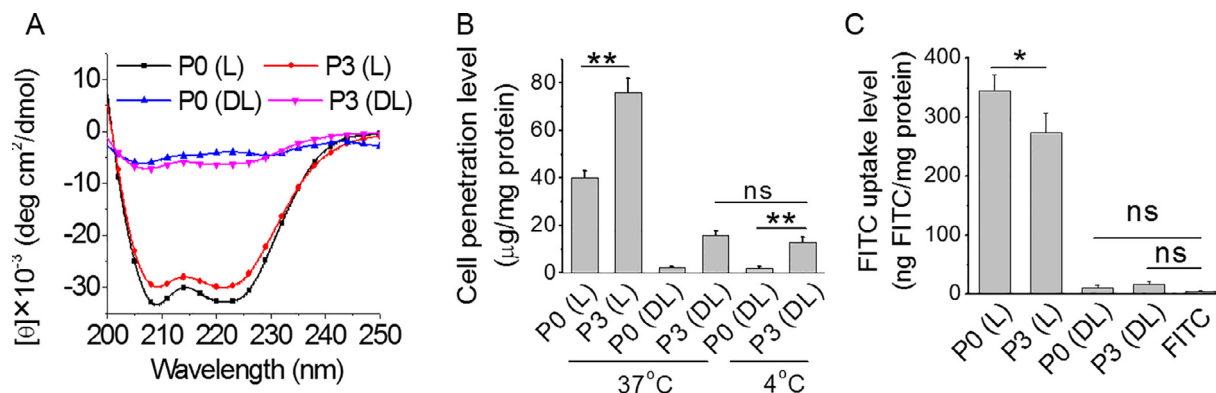


Fig. 2. (A) CD spectra of **P0** and **P3** with different α -carbon stereochemistry in DI water at pH 7 (0.1 mg/mL). (B) Cell penetration levels of RhB-**P0** and RhB-**P3** in both helical and random coiled conformation in HeLa cells at both 37 °C and 4 °C (n = 3). (C) FITC-Tris uptake level in HeLa cells following co-incubation with **P0** and **P3** in both helical and random coiled conformation for 4 h at 37 °C (n = 3).

DNA, nano-scale complexes (~ 150 nm) with positive zeta potential ($\sim +30$ mV) were obtained (Supplementary Fig. S5). pDNA was then labeled with YOYO-1 and allowed to form complexes with polypeptides, and the capability of polypeptide to mediate intracellular DNA delivery was evaluated in HeLa cells following 4-h incubation. As shown in Fig. 3A, the aromatic polypeptides featured stronger potency than the un-modified **P0** in promoting intracellular delivery of pDNA, and the top-performing **P3** bearing 20 mol% of naphthyl side chains showed the highest DNA uptake

level which was three fold higher than **P0**. Such tendency accorded well with the membrane penetration activities of the polypeptides (Fig. 1C). When incubated at 4 °C, the DNA uptake level mediated by aromatic polypeptides (**P1–P6**) was inhibited by $\sim 40\%$ in comparison to the 70% inhibition level for the unmodified **P0**, further demonstrating that aromatic domains on polypeptide side chains promoted the non-endocytic delivery of DNA cargos into cells. To further evaluate the endosomal escape mediated by the aromatic polypeptides, we visualized the intracellular distribution of

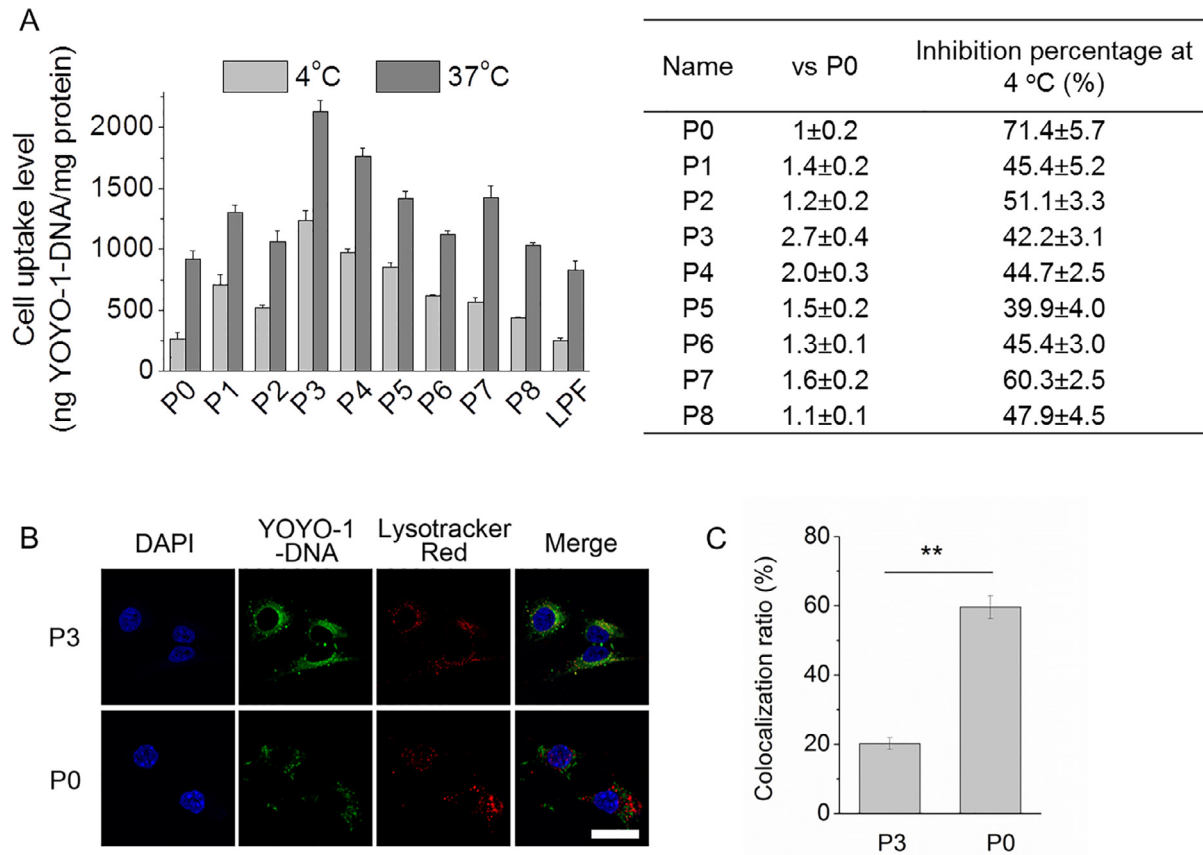


Fig. 3. (A) Uptake level of complexes containing YOYO-1-DNA in HeLa cells following incubation for 4 h at 4 °C and 37 °C (left), fold of increment over **P0** (right), and inhibition percentage at 4 °C (right) (n = 3). (B) CLSM images of HeLa cells treated with **P3**/YOYO-1-DNA and **P0**/YOYO-1-DNA complexes for 4 h. Blue, DAPI-stained nuclear. Green, YOYO-1 stained DNA. Red, Lysotracker Red stained endosome/lysosome. Bar represents 20 μ m. (C) Colocalization ratio of YOYO-1-DNA with Lysotracker Red-stained endosomes (n = 20). (For interpretation of the references to colour in this figure legend, the reader is referred to the web version of this article.)

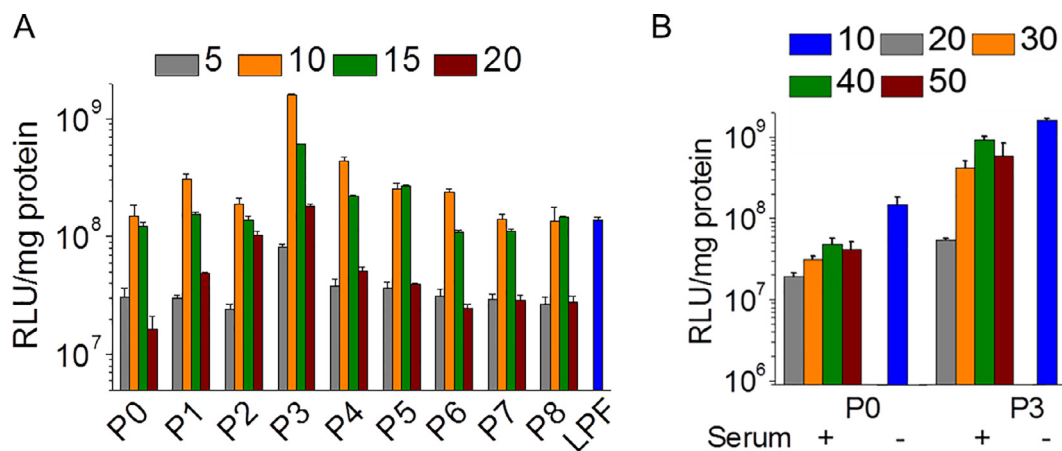


Fig. 4. (A) Transfection efficiencies of **P0** to **P8** in HeLa cells at various polymer/DNA weight ratios in the absence of serum (n = 3). (B) Comparison of the transfection efficiencies of **P0** and **P3** in HeLa cells at various polymer/DNA weight ratios in the absence or presence of 10% serum (n = 3).

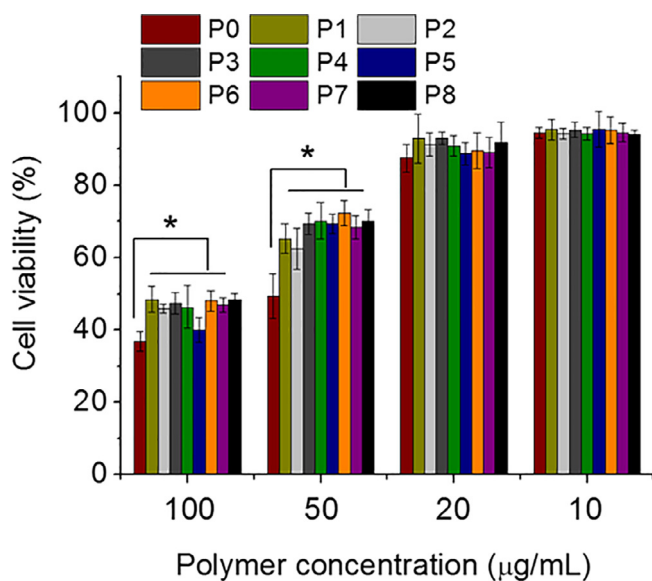


Fig. 5. Cytotoxicity of **P0** to **P8** following 24-h incubation in HeLa cells as determined by the MTT assay (n = 3).

YOYO-1-DNA and its colocalization with LysoTracker Red-stained endosomes by CLSM (Fig. 3B). Greater separation between red fluorescence (LysoTracker Red) and green fluorescence (YOYO-1-DNA)

was noted for the aromatic polypeptide **P3** compared to the non-modified **P0**, substantiated that the non-endocytic, direct translocation of gene cargoes mediated by the aromatic polypeptide effectively avoided the entrapment by endosomes, a critical barrier against effective gene transfection. Such findings were further supported by the quantitative analysis of CLSM images which revealed significantly lower colocalization ratio between green and red fluorescence for **P3** than for **P0** (Fig. 3C).

We next investigated the *in vitro* gene transfection efficiencies in HeLa cells. Under serum-free conditions, enhanced luciferase expression levels were noted for polypeptides modified with phenyl and naphthyl groups (**P1–P4**), and an increased aromatic content from 20 to 50 mol% led to decreased transfection efficiencies that were consistent with their aromaticity-associated membrane activities (Fig. 4A). **P3** that afforded the strongest membrane penetration capabilities also enabled the highest transfection efficiency, which was 10.7 and 11.5 fold higher than **P0** and commercial transfection reagent Lipofectamine 2000 (LPF), respectively. In the presence of 10% serum, the transfection efficiencies of **P0** was dramatically decreased by ~80% in comparison to the ~30% reduction for **P3** (Fig. 4B), which indicated that aromatic modification enhanced the resistance of polypeptide/DNA complexes against serum. Such enhanced serum resistance could be presumably attributed to the decreased positive charge densities and the presence of aromatic domains that inhibited protein binding onto polyplex surfaces, and thus provided desired advantages for effective *in vivo* gene delivery that is often compromised by the pres-

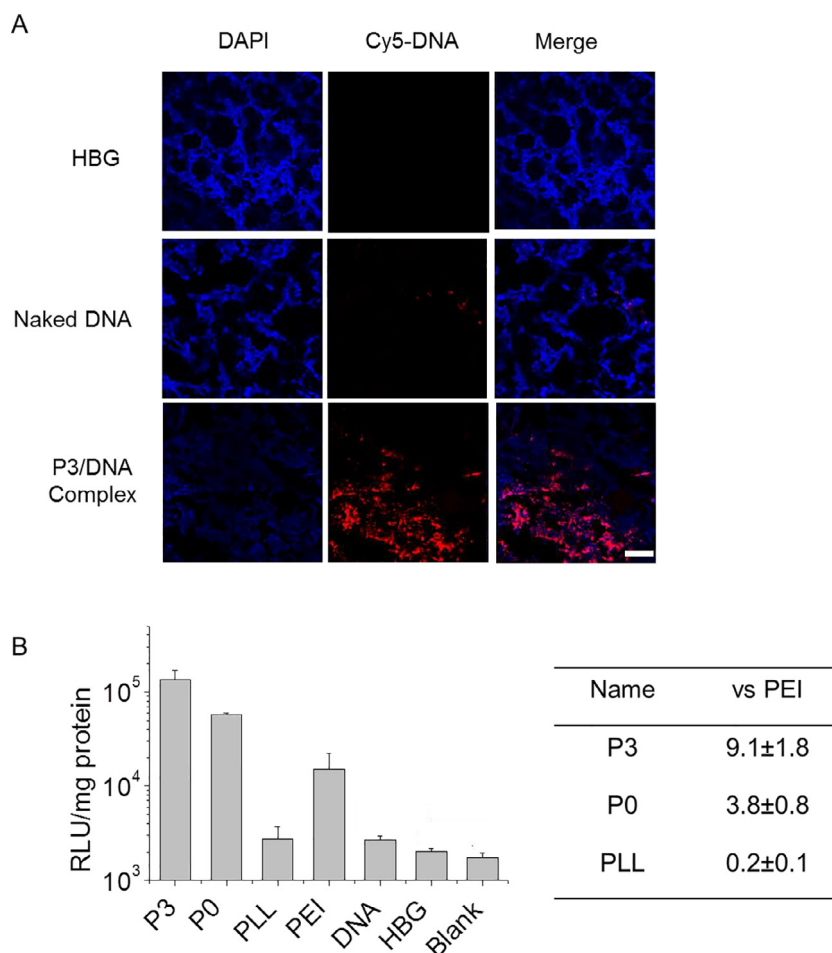


Fig. 6. (A) CLSM images of melanoma tissues following intratumoral injection of naked Cy5-DNA and **P3**/Cy5-DNA polyplexes. Red, Cy5-DNA. Blue, DAPI-stained nuclear. Bar represents 50 µm. (B) *In vivo* transfection efficiencies of **P3**/DNA polyplexes, PLL/DNA polyplexes, PEI/DNA complexes, free DNA, and free buffer solutions following intratumoral injections in B16F10 xenograft tumor-bearing C57BL6 mice at 30 µg DNA/mouse (n = 4).

ence of serum [41,42]. The enhanced transfection efficiencies under both serum-free and serum-containing conditions were further substantiated in B16F10 cells (Supplementary Fig. S6).

3.4. Cytotoxicity of aromatic polypeptides

The transfection efficiency and cytotoxicity of polycations, including the cationic helical polypeptides, are often inversely correlated [43,44]. Cationic polypeptides with higher charge density often afford stronger DNA condensation capacities, higher membrane activities as well as transfection efficiencies. However, they also induce severe cytotoxicities when excessive membrane activities are imposed. Therefore, optimal balance between the membrane activity and cytotoxicity is of particular importance during the design of gene vectors. As indicated by Fig. 5, all the aromatically modified polypeptides (P1–P6) demonstrated lower cytotoxicities than the unmodified P0 toward HeLa cells, which could be mainly attributed to the reduced cationic charge densities on polypeptide side chains that diminished the charge-induced irreversible membrane damage. Similar trend was also noted for polypeptide/DNA complexes following incubation with HeLa cells for 24 h (Supplementary Fig. S7). More importantly, P3 showed notably lower cytotoxicity than PEI as a widely used transfection reagent (Supplementary Fig. S8), which clearly verified its advantage over existing gene delivery systems.

3.5. *In vivo* gene delivery in melanoma-bearing mice

P3, the top-performing polypeptide identified above in terms of the *in vitro* transfection efficiency, was further explored for its capability to mediate *in vivo* transfection in melanoma-bearing mice following intratumoral injection. Polyplexes containing Cy5-labeled DNA were first injected and the intracellular distribution of Cy5-DNA was visualized 4 h later. As shown in Fig. 6A, extensive Cy5 fluorescence was distributed in the tumor cells and cell nuclei after intratumoral injection of P3/Cy5-DNA polyplexes, while negligible Cy5 fluorescence was noted for naked DNA, which verified that P3 was able to efficiently deliver plasmid DNA into melanoma tumor cells *in vivo*. As shown in Fig. 6B, the aromatically modified P3 afforded higher transfection efficiencies than the unmodified P0, poly(L-lysine) (PLL), and commercial transfection reagent PEI (25 kDa) in terms of enhanced luciferase expression levels at 48 h post intratumoral injection at 30 µg pCMV-Luc/mouse, which could be attributed to the collective outcomes of aromatic domain-strengthened membrane activities and serum resistance of helical polypeptide/DNA complexes. With its higher transfection efficiencies while lower toxicities than commercial reagent PEI, the aromatically modified helical polypeptide holds potentials as a promising addition to existing systems toward topical gene delivery for cancer therapy.

4. Conclusion

In conclusion, we have developed aromatically modified, cationic, α -helical polypeptides which afford superior membrane activities as well as gene delivery efficiencies. More importantly, we unraveled that the incorporation of aromatic domains significantly altered their membrane penetration mechanisms to promote the non-endocytic internalization of gene cargos via direct membrane transduction rather than the pore formation mechanism. As a consequence, the endosomal entrapment of cargos could be avoided and the material toxicity could be reduced. The aromatic motifs also enhanced the resistance against serum, leading to efficient gene transfection under serum-containing conditions. This study provides a promising mechanism-driven structural design strategy

which manipulates the membrane penetration mechanisms of helical polypeptides to overcome the multiple critical barriers against non-viral gene delivery. The aromatic polypeptides with desired transfection efficiencies in melanoma cells *in vitro* and *in vivo* also hold promising potentials toward the topical gene delivery for cancer therapy.

Acknowledgements

L. Y. acknowledges the support from the National Natural Science Foundation of China (51403145 and 51573123), the Ministry of Science and Technology of China (2016YFA0201200), the Science and Technology Department of Jiangsu Province (BK20140333), and Priority Academic Program Development of Jiangsu Higher Education Institutions (PAPD). J.C. acknowledges support from the NSF (CHE-1153122) and the NIH (NIH Director's New Innovator Award 1DP2OD007246 and 1R21EB013379).

Appendix A. Supplementary data

Supplementary data associated with this article can be found, in the online version, at <http://dx.doi.org/10.1016/j.actbio.2017.05.001>.

Reference

- [1] F. McCormick, Cancer gene therapy: fringe or cutting edge?, *Nat. Rev. Cancer* 1 (2001) 130–141.
- [2] A. de Fougères, H.-P. Vornlocher, J. Maraganore, J. Lieberman, Interfering with disease: a progress report on siRNA-based therapeutics, *Nat. Rev. Drug Discov.* 6 (2007) 443–453.
- [3] M. Candolfi, W. Xiong, K. Yagci, C. Liu, A.K.M.G. Muhammad, M. Puntel, D. Foulad, A. Zadmehr, G.E. Ahlzadeh, K.M. Kroeger, M. Tesarfreund, S. Lee, W. Debinski, D. Sareen, C.N. Svendsen, R. Rodriguez, P.R. Lowenstein, M.G. Castro, Gene therapy-mediated delivery of targeted cytotoxins for glioma therapeutics, *Proc. Natl. Acad. Sci. USA* 107 (2010) 20021–20026.
- [4] M.A. Islam, E.K.G. Reesor, Y.J. Xu, H.R. Zope, B.R. Zetter, J.J. Shi, *Biomaterials for mRNA delivery*, *Biomater. Sci.* 3 (2015) 1519–1533.
- [5] A.M. Grabowska, R. Kircheis, R. Kumari, P. Clarke, A. McKenzie, J. Hughes, C. Mayne, A. Desai, L. Sasso, S.A. Watson, C. Alexander, Systemic *in vivo* delivery of siRNA to tumours using combination of poly(ethyleneimine) and transferrin-polyethyleneimine conjugates, *Biomater. Sci.* 3 (2015) 1439–1448.
- [6] G.J. Hannon, RNA interference, *Nature* 418 (2002) 244–251.
- [7] M.E. Davis, J.E. Zuckerman, C.H.J. Choi, D. Seligson, A. Tolcher, C.A. Alabi, Y. Yen, J.D. Heide, A. Ribas, Evidence of RNAi in humans from systemically administered siRNA via targeted nanoparticles, *Nature* 464 (2010) 1067–1070.
- [8] M. Wang, K. Alberti, A. Varone, D. Pouli, I. Georgakoudi, Q.B. Xu, Enhanced intracellular siRNA delivery using bioreducible lipid-like nanoparticles, *Adv. Healthc. Mater.* 3 (2014) 1398–1403.
- [9] C.E. Thomas, A. Ehrhardt, M.A. Kay, Progress and problems with the use of viral vectors for gene therapy, *Nat. Rev. Genet.* 4 (2003) 346–358.
- [10] M. Morille, C. Passirani, A. Vonarbourg, A. Clavreul, J.-P. Benoit, Progress in developing cationic vectors for non-viral systemic gene therapy against cancer, *Biomaterials* 29 (2008) 3477–3496.
- [11] J.K.Y. Tan, J.L. Choi, H. Wei, J.G. Schellinger, S.H. Pun, Reducible, dibromomaleimide-linked polymers for gene delivery, *Biomater. Sci.* 3 (2015) 112–120.
- [12] A. Mangraviti, S.Y. Tzeng, K.L. Kozielski, Y. Wang, Y.K. Jin, D. Gullotti, M. Pedone, N. Buaron, A. Liu, D.R. Wilson, S.K. Hansen, F.J. Rodriguez, G.D. Gao, F. DiMeco, H. Brem, A. Olivi, B. Tyler, J.J. Green, Polymeric nanoparticles for nonviral gene therapy extend brain tumor survival *in vivo*, *ACS Nano* 9 (2015) 1236–1249.
- [13] C. Zhang, R. Jin, P. Zhao, C. Lin, A family of cationic polyamides for *in vitro* and *in vivo* gene transfection, *Acta Biomater.* 22 (2015) 120–130.
- [14] M. Keeney, S.G. Ong, A. Padilla, Z.Y. Yao, S. Goodman, J.C. Wu, F. Yang, Development of poly(beta-amino ester)-based biodegradable nanoparticles for nonviral delivery of minicircle DNA, *ACS Nano* 7 (2013) 7241–7250.
- [15] S. Siegmán, N. Truong, T. Segura, Encapsulation of PEGylated low-molecular-weight PEI polyplexes in hyaluronic acid hydrogels reduces aggregation, *Acta Biomater.* 28 (2015) 45–54.
- [16] M. Keeney, S. Onyiah, Z. Zhang, X.M. Tong, L.H. Han, F. Yang, Modulating polymer chemistry to enhance non-viral gene delivery inside hydrogels with tunable matrix stiffness, *Biomaterials* 34 (2013) 9657–9665.
- [17] F.C. Pérez-Martínez, J. Guerra, I. Posadas, V. Ceña, Arriers to non-viral vector-mediated gene delivery in the nervous system, *Pharmaceut. Res.* 28 (2011) 1843–1858.
- [18] M. Lindgren, M. Hällbrink, A. Prochiantz, Ü. Langel, Cell-penetrating peptides, *Trends Pharmacol. Sci.* 21 (2000) 99–103.

- [19] S.B. Fonseca, M.P. Pereira, S.O. Kelley, Recent advances in the use of cell-penetrating peptides for medical and biological applications, *Adv. Drug Deliver. Rev.* 61 (2009) 953–964.
- [20] C.B. Park, K.-S. Yi, K. Matsuzaki, M.S. Kim, S.C. Kim, Structure–activity analysis of buforin II, a histone H2A-derived antimicrobial peptide: the proline hinge is responsible for the cell-penetrating ability of buforin II, *Proc. Natl. Acad. Sci. USA* 97 (2000) 8245–8250.
- [21] D.S. Daniels, A. Schepartz, Intrinsically cell-permeable miniature proteins based on a minimal cationic PPII motif, *J. Am. Chem. Soc.* 129 (2007) 14578–14579.
- [22] G. Ter-Avetisyan, G. Tünnemann, D. Nowak, M. Nitschke, A. Herrmann, M. Drab, M.C. Cardoso, Cell entry of arginine-rich peptides is independent of endocytosis, *J. Biol. Chem.* 284 (2009) 3370–3378.
- [23] J.G. Schellinger, J.A. Pahang, R.N. Johnson, D.S.H. Chu, D.L. Sellers, D.O. Maris, A. J. Convertine, P.S. Stayton, P.J. Horner, S.H. Pun, Melittin-grafted HPMA-oligolysine based copolymers for gene delivery, *Biomaterials* 34 (2013) 2318–2326.
- [24] P.E. Saw, Y.T. Ko, S. Jon, Efficient liposomal nanocarrier-mediated oligodeoxynucleotide delivery involving dual use of a cell-penetrating peptide as a packaging and intracellular delivery agent, *Macromol. Rapid Commun.* 31 (2010) 1155–1162.
- [25] H. Tang, L. Yin, K.H. Kim, J. Cheng, Helical poly(arginine) mimics with superior cell-penetrating and molecular transporting properties, *Chem. Sci.* 4 (2013) 3839–3844.
- [26] N.P. Gabrielson, H. Lu, L. Yin, D. Li, F. Wang, J. Cheng, Reactive and bioactive cationic α -helical polypeptide template for nonviral gene delivery, *Angew. Chem. Int. Ed.* 124 (2012) 1169–1173.
- [27] H. Lu, J. Wang, Y. Bai, J.W. Lang, S. Liu, Y. Lin, J. Cheng, Ionic polypeptides with unusual helical stability, *Nat. Commun.* 2 (2011) 206.
- [28] L. Yin, H. Tang, K.H. Kim, N. Zheng, Z. Song, N.P. Gabrielson, H. Lu, J. Cheng, Light-responsive helical polypeptides capable of reducing toxicity and unpacking DNA: toward nonviral gene delivery, *Angew. Chem. Int. Ed.* 52 (2013) 9182–9186.
- [29] X. Lu, F. Jia, X. Tan, D. Wang, X. Cao, J. Zheng, K. Zhang, Effective antisense gene regulation via noncationic, polyethylene glycol brushes, *J. Am. Chem. Soc.* 138 (2016) 9097–9100.
- [30] A. Verma, O. Uzun, Y. Hu, Y. Hu, H.-S. Han, N. Watson, S. Chen, D.J. Irvine, F. Stellacci, Surface-structure-regulated cell-membrane penetration by monolayer-protected nanoparticles, *Nat. Mater.* 7 (2008) 588–595.
- [31] P. Guterstam, F. Madani, H. Hirose, T. Takeuchi, S. Futaki, S. El Andaloussi, A. Gräslund, Ü. Langel, Elucidating cell-penetrating peptide mechanisms of action for membrane interaction, cellular uptake, and translocation utilizing the hydrophobic counter-anion pyrenebutyrate, *Biochim. Biophys. Acta* 1788 (2009) 2509–2517.
- [32] A. Som, A. Reuter, G.N. Tew, Protein transduction domain mimics: the role of aromatic functionality, *Angew. Chem. Int. Ed.* 51 (2012) 980–983.
- [33] A. Som, A.O. Tezgel, G.J. Gabriel, G.N. Tew, Self-activation in de novo designed mimics of cell-penetrating peptides, *Angew. Chem. Int. Ed.* 50 (2011) 6147–6150.
- [34] E.I. Geihe, C.B. Cooley, J.R. Simon, M.K. Kiesewetter, J.A. Edward, R.P. Hickerson, R.L. Kaspar, J.L. Hedrick, R.M. Waymouth, P.A. Wender, Designed guanidinium-rich amphipathic oligocarbonate molecular transporters complex, deliver and release siRNA in cells, *Proc. Natl. Acad. Sci. USA* 109 (2012) 13171–13176.
- [35] F. Perret, M. Nishihara, T. Takeuchi, S. Futaki, A.N. Lazar, A.W. Coleman, N. Sakai, S. Matile, Anionic fullerenes, calixarenes, coronenes, and pyrenes as activators of oligo/polyarginines in model membranes and live cells, *J. Am. Chem. Soc.* 127 (2005) 1114–1115.
- [36] C.E.B. Caesar, E.K. Esbjörner, P. Lincoln, B. Nordén, Membrane interactions of cell-penetrating peptides probed by tryptophan fluorescence and dichroism techniques: correlations of structure to cellular uptake, *Biochemistry* 45 (2006) 7682–7692.
- [37] H. Lu, Y. Bai, J. Wang, N.P. Gabrielson, F. Wang, Y. Lin, J. Cheng, Ring-opening polymerization of gamma-(4-vinylbenzyl)-(L)-glutamate N-carboxyanhydride for the synthesis of functional polypeptides, *Macromolecules* 44 (2011) 6237–6240.
- [38] B.R. McNaughton, J.J. Cronican, D.B. Thompson, D.R. Liu, Mammalian cell penetration, siRNA transfection, and DNA transfection by supercharged proteins, *Proc. Natl. Acad. Sci. USA* 106 (2009) 6111–6116.
- [39] H. He, N. Zheng, Z. Song, K.H. Kim, C. Yao, R. Zhang, C. Zhang, Y. Huang, F.M. Uckun, J. Cheng, Y. Zhang, L. Yin, Suppression of hepatic inflammation via systemic siRNA delivery by membrane-disruptive and endosomolytic helical polypeptide hybrid nanoparticles, *ACS Nano* 10 (2016) 1859–1870.
- [40] Y. Shai, Z. Oren, *Peptides* 22 (2001) 1629–1641.
- [41] M.C. Morris, E. Gros, G. Aldrian-Herrada, M. Choo, J. Archdeacon, F. Heitz, G. Divita, A non-covalent peptide-based carrier for in vivo delivery of DNA mimics, *Nucleic Acids Res.* 35 (2007) e49.
- [42] Y. Wang, J. Li, Y. Chen, D. Oupicky, Balancing polymer hydrophobicity for ligand presentation and siRNA delivery in dual function CXCR4 inhibiting polyplexes, *Biomater. Sci.* 3 (2015) 1114–1123.
- [43] N. Zheng, L. Yin, Z. Song, L. Ma, H. Tang, N.P. Gabrielson, H. Lu, J. Cheng, Maximizing gene delivery efficiencies of cationic helical polypeptides via balanced membrane penetration and cellular targeting, *Biomaterials* 35 (2014) 1302–1314.
- [44] M. Hellmund, K. Achazi, F. Neumann, B.N.S. Thota, N. Ma, R. Haag, Systematic adjustment of charge densities and size of polyglycerol amines reduces cytotoxic effects and enhances cellular uptake, *Biomater. Sci.* 3 (2015) 1459–1465.